8.A.1

Nuclear Physics B33 (1971) 253–280. North-Holland Publishing Company

ISOSPIN INVARIANCE IN THE REACTION np → π^0d *

S.S.WILSON**, M.J.LONGO and K.K.YOUNG***
University of Michigan, Ann Arbor, Michigan 48104, USA

and

J.A.HELLAND‡ and B.L.SCHROCK
University of California, Los Angeles, California 90024, USA

Received 15 February 1971
(Revised 5 July 1971)

Abstract: A measurement of the differential cross section for the reaction np → π^0d has been made at the Lawrence Radiation Laboratory 184-inch cyclotron. A neutron beam with kinetic energies up to 720 MeV was incident on a liquid hydrogen target. The angle and momentum of the deuterons were measured using an analyzing magnet and wire spark chambers with a magnetostrictive readout. Deuterons were separated from protons by time-of-flight. The photons from the decaying π^0 were not detected. The neutron energy was calculated from the measured deuteron angle and momentum.

Out of 5 × 10^5 events recorded, 1.1 × 10^5 events were the desired π^0d reaction. The cross sections were compared to those for the reaction π^+d → pp as a test of isotopic spin invariance in strong interactions. The symmetry of the cross sections about 90° was also investigated, and an upper limit of about 1% was placed on the real part of the ratio of isospin-violating to isospin-conserving amplitudes.

1. INTRODUCTION

In this report we describe an experimental study of the reaction np → π^0d and its significance as a test of isotopic spin invariance in strong interactions. These data were obtained in conjunction with an experiment whose primary objective was to test time reversal invariance in the photodisintegration of the deuteron by measuring cross sections for the reaction np → γd [1]; but, with little extra effort, about

* Supported by the National Science Foundation and the US Atomic Energy Commission.
** Now at Bendix Aerospace Systems Division, Ann Arbor, Michigan.
*** Now at University of Washington, Seattle, Washington.
‡ Now at Lawrence Radiation Laboratory, Berkeley, California.

5×10^5 events were recorded to obtain cross sections for $np \to \pi^0 d$ from threshold to 720 MeV incident neutron energy. The experiments were carried out at the Lawrence Radiation Laboratory (LRL) 184-inch cyclotron.

The cross section for $\pi^0 d$ production is about 100 times larger than that for γd production. To discriminate between these two reactions in the γd experiment the deuteron angle and momentum were measured using spark chambers and a magnetic spectrometer, and also the gamma angle was measured using shower chambers. The gamma chamber array also detected gammas coming from the decaying π^0 from the $\pi^0 d$ reaction. In the data analysis the two reactions could be separated using kinematics to distinguish γd production from $\pi^0 d$ production. It would have been possible to obtain the $\pi^0 d$ cross section simply by using the enormous number of events rejected in the γd experiment. This was not done because the gamma chambers were not necessary for the $\pi^0 d$ cross section determination. Inclusion of the gamma chambers would have made the data analysis much more difficult. The calculation of the solid angle of the detectors would have required an accurate and extensive Monte Carlo calculation. We would also have needed a detailed knowledge of the efficiency of the gamma detector down to about 50 MeV.

It was much easier to obtain the $d\pi^0$ cross section by making separate runs where the gamma chambers were not used, and the event was recorded when only a deuteron was detected. The total event rate in this mode was as high as five events per second and was limited only by the recovery time of the spark chambers. The total running time to obtain the $\pi^0 d$ data was about four days. With the simple trigger logic used, about half the events were protons coming from elastic and inelastic collisions rather than deuterons. For particles of the same momentum, the time-of-flight information (recorded with a time-to-height system) was used to separate the deuterons from the faster moving protons.

As pointed out by Yang in 1952 isotopic spin invariance requires that the cross section for the reaction $np \to \pi^0 d$ must be half of that for $pp \to \pi^+ d$, i.e.,

$$\frac{\sigma(pp \to \pi^+ d)}{\sigma(np \to \pi^0 d)} = 2 . \tag{1}$$

This can be shown by expressing the initial and final states as eigenstates of total isospin

$$\frac{\sigma(pp \to \pi^+ d)}{\sigma(np \to \pi^0 d)} = \frac{|\langle 1,1|S|1,1\rangle|^2}{|1/\sqrt{2}\langle 1,0|S|1,0\rangle + 1/\sqrt{2}\langle 1,0|S|0,0\rangle|^2} , \tag{2}$$

where S is the scattering matrix. If isospin is conserved the second term in the denominator must vanish. Strong forces are independent of the third component of isospin, so

$$\langle 1,1|S|1,1\rangle = \langle 1,0|S|1,0\rangle ,$$

and the amplitudes in the numerator and denominator cancel leaving a factor of two.

There are three consequences of isospin invariance which we specifically investigate:

(1) Our angular distributions should be symmetric about 90° as are those for $pp \to \pi^+ d$, (because of the identity of the two protons in the initial state). Thus we check for an asymmetry of our angular distributions about 90°. This test does not require knowledge of the results of other $NN \rightleftharpoons \pi^+ d$ experiments.

This test is sensitive to the requirement that total isospin is conserved; namely $\langle 1,0|S|0,0\rangle = 0$ in eq. (2). If this amplitude were not zero, it would give rise to odd powers of $\cos\theta$ in the angular distribution, whereas the allowed $\langle 1,0|S|1,0\rangle$ transition gives rise only to even powers of $\cos\theta$.

(2) The shape of the angular distribution for $np \to \pi^0 d$ should be the same as that for $pp \to \pi^+ d$. Thus we fit our angular distributions to the function

$$\sigma(\theta) \propto A + \cos^2\theta^* + B\cos^4\theta^* ,$$

and compare the values of A and B with those for $pp \to \pi^+ d$ from other experiments. This check depends on the relation

$$\langle 1,1|S|1,1\rangle = \langle 1,0|S|1,0\rangle ,$$

and is therefore sensitive to a violation of the invariance of the strong interaction with respect to I_3.

(3) The total cross section for our experiment should be one-half that for $pp \to \pi^+ d$ at all energies. We have made this check, but it is not very accurate.

These three checks could show violations due to the electromagnetic interaction, but we know of no theoretical work done to calculate the size and nature of the EM violation in this reaction. Furthermore the EM violation would be expected to be small since there are no Coulomb forces in either the initial or final states of the reaction $np \to \pi^0 d$ and the EM mass differences are small relative to the incident energy. We have not seen a violation in this experiment even at the 1% level, so the size of the EM violation is still unknown.

Tests of isospin violation in other types of experiments are often more difficult because the EM corrections are considerably larger, typically ranging from 2 to 10%. The investigation of bound states to test isospin is difficult because of the large Coulomb corrections which are necessary.

Isospin invariance requires that the total cross section the scattering of a π^- off of a deuteron should be the same as that for a π^+. The total cross sections have been measured to be equal within about 1% [2,3] over a large energy range. However this method only checks invariance with respect to the I_3 component; it does not check conservation of total isospin.

A number of experiments have been done involving pions and light nuclei. The reaction

$$dd \rightarrow He^4\pi^0$$

is forbidden because of isospin invariance. (The deuteron and He^4 have zero isospin whereas the pion has isospin one.) An upper limit for the cross section has been measured by Poirier and Pripstein [4]. Greider [5] calculated from these results that isospin is conserved to at least 6.5%.

Isospin invariance requires that the cross section for

$$pd \rightarrow \pi^+H^3 , \qquad pd \rightarrow \pi^0He^3$$

should have the ratio

$$\frac{\sigma(H^3)}{\sigma(He^3)} = 2 .$$

These reactions were measured by Crewe et al. [6] at 450 MeV, and by Hartig et al. [7] at 591 MeV respectively. This test involves a rather large and uncertain EM correction of about 6% since there is a large difference between the wave functions of H^3 and He^3.

2. EXPERIMENTAL APPARATUS

A floor plan of the experiment is shown in fig. 1. A beryllium target 10.0 cm long and 1.3 cm square inside the cyclotron served as an internal target to create neutrons. The neutrons that came off at approximately zero degrees with respect to the bombarding protons passed through collimators totaling 4.2 m of steel in length. The defining aperture was 3.8 cm in diameter 5 m from the target. Charged particles formed in the internal target were swept away from the collimator by the magnetic field of the cyclotron. Most of the gamma rays in the beam were eliminated by a lead γ converter 5 cm thick.

Charged particles created in the collimator were removed by a sweeping magnet downstream of the last collimator. The neutrons passed through a liquid hydrogen target and then through beam monitor counters. The beam at the hydrogen target had a diameter of approximately 5 cm and an intensity $\sim 4 \times 10^6$ neutrons/sec. The duty cycle of the cyclotron was about 50%.

The deuterons were detected by a coincidence between counters D_1 and D_2. The time delay of the pulses from D_1 and D_2 was carefully adjusted to accept all deuterons in the desired momentum range and reject as many of the faster moving protons as possible. The orbits were recorded by using four spark chambers with a magnetostrictive readout system. The analyzing magnet was mounted on a swivel mount and tracks so that its position would easily be changed.

An on-line PDP-5 computer and magnetic tape unit was used to continuously

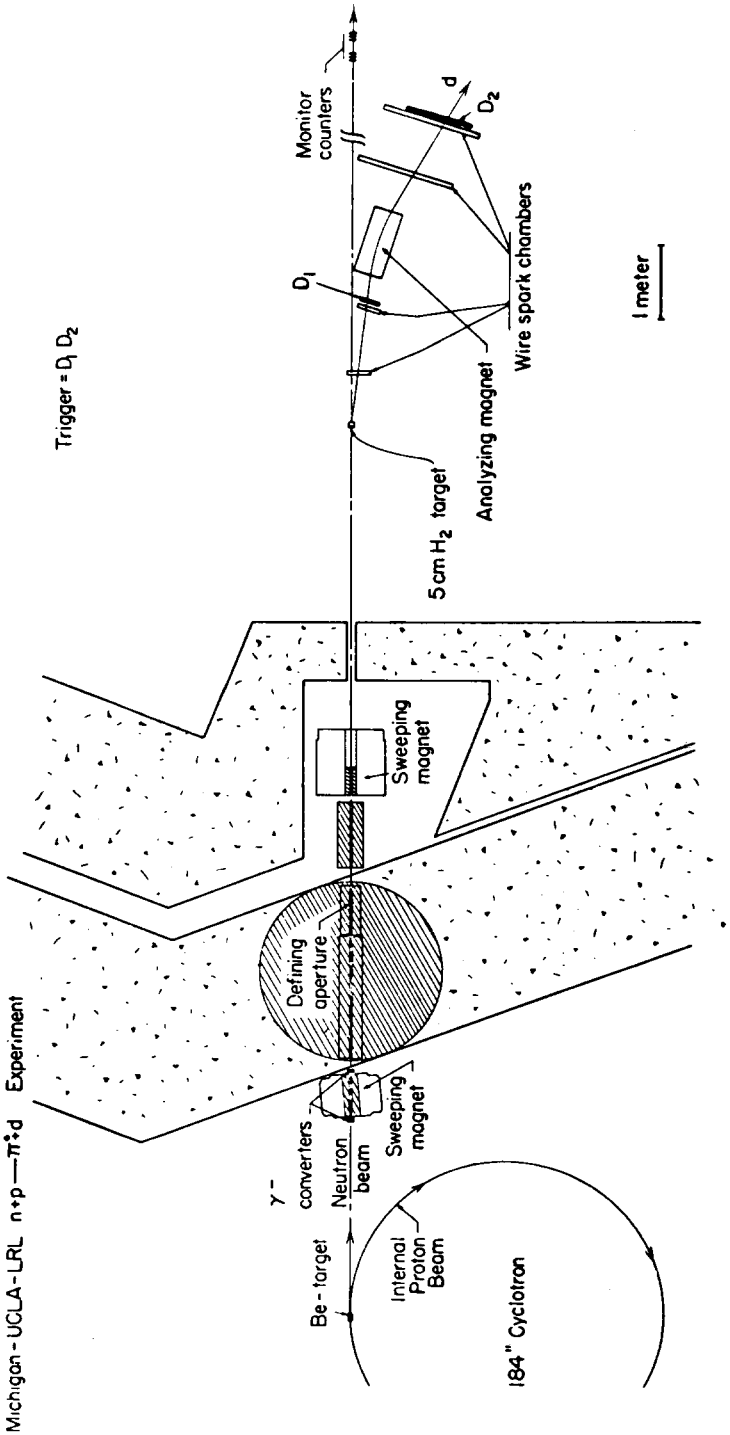

Fig. 1. Layout of experiment.

monitor the experiment and record the digitized spark coordinate readings, beam monitor counters, and time of flight between D_1 and D_2.

The absolute flux of neutrons in the beam as a function of energy was determined from the np → γd data [1]. It was obtained by assuming detailed balance and using the total cross sections measured in γd → np experiments. The number of γd events in a particular energy range (after accounting for efficiencies) was divided by the cross section to obtain the relative number of neutrons. The resulting neutron distribution is shown in fig. 2. There are large uncertainties in the total cross section measurements in the γd → np experiments. This will result in an equally large uncertainty in the neutron energy distribution.

The spatial distribution of neutrons in the beam was found by projecting the deuteron orbits from the first two chambers back to the target midplane to find the projected interaction point in the target. The distribution of the target interaction points should be the same as the spatial distribution of the neutron beam for a target of uniform thickness. The measured distribution was found to be a function of radius only and is shown in fig. 3. It is slightly smeared out by the finite target length and Coulomb scattering of the deuterons.

The neutron beam intensity was continually monitored by three identical sets of three monitor counters for reliability and redundancy (fig. 1). The first in each set was an anticounter which insured that the second two counters were not counting charged particles in the beam. A polyethylene block after the first counter created charged particles which the second and third counters detected in coincidence. The three sets of counters tracked to within 1% of each other during the experiment.

The liquid hydrogen was contained in a cylinder 7.5 cm in diameter and approximately 5.5 cm long with the axis of the cylinder along the incident beam direction. The material in the beam was minimized to reduce interactions in the target walls and Coulomb scattering. There was 0.44 g/cm^2 of hydrogen in the target and 0.03 g/cm^2 of mylar.

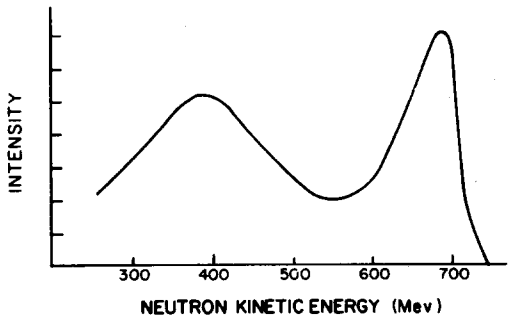

Fig. 2. Neutron energy distribution in beam as determined from np → γd yields and detailed balance. The uncertainty in the γd → np total cross sections lead to uncertainties ~ ± 30% in the energy distribution.

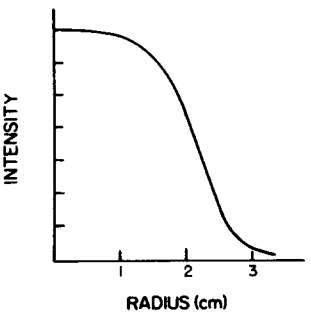

Fig. 3. Beam profile (number of neutrons/cm^2 versus radius).

The momentum analyzing magnet was a forty ton "C" magnet with a rectangular pole face 91.4 by 40.6 cm and a gap 20.3 cm high. The LRL magnet group measured the vertical component of the field at 5151 different points in a lattice of 79 X 29 X 3 points along the length, width, and vertical directions respectively. These measurements were made for six different currents ranging from 980 to 2000 amps, corresponding to central fields which range from 10.5 to 17.6 kG.

Each spark chamber consisted of four planes of closely spaced wires with one plane in each chamber oriented along the horizontal and vertical directions and the other two at ±45°. The first two chambers had an active area of 25 cm square. The frames were made of lucite and the "wires" were 0.5 mm wide by 0.025 mm thick aluminum ribbons on a mylar sheet 0.05 mm thick. Printed circuit techniques were used to etch the grid of wires out of aluminized mylar. The third and fourth chambers had an active area 45 by 55 cm. They were constructed of 0.15 mm aluminum wires spaced 1 mm apart and glued to an epoxy-fiberglass frame. On all the chambers slots were milled in the frames so that a magnetostrictive wire mounted on an aluminum bar could be slid in to sense the location of the wire(s) which were sparked. Wires at each end of the planes were also pulsed every time the chamber was pulsed to provide start and stop fiducials for the readout electronics. Details of the spark chambers and magnetostrictive readout system are given in ref. [8].

Deuterons from π^0d production come from the target at lab angles from 0° to 14° with momenta from 675 to 1500 MeV/c. In order to span the deuteron angles and momenta of interest, 9 magnet settings with different currents and positions were used. The magnet was moved to three positions in order to cover the angular region. The first position covered angles from 0° to 6.5°. The second covered 5.25° to 10.0°; and the third covered 8.0° to 14.0°. For each of these positions, different current settings were used to cover the momentum space.

Aside from the beam monitor counters, only three other counters were used in this experiment. They were constructed of Pilot B plastic scintillator and were located as shown in fig. 1. D_1 had dimensions 20 X 25 X 0.15 cm thick. An anti-counter A_1 was used to effectively reduce the size of D_1 to limit the angular acceptance of deuterons. It was located just in front of D_1. D_2 was 30 X 55 X 0.6 cm thick. These counters were coupled to 56AVP photomultiplier tubes with lucite light pipes.

The event trigger was simply $D_1 D_2 \bar{A}_1$. Pulses from D_1 and D_2 were also sent to a module which digitized the time difference to an accuracy of $\pm\frac{1}{2}$ nsec. The event trigger enabled the readout electronics and started a 200 msec gate which turned off the whole system to allow the spark chambers to recover. Data taking rates were typically four events per second.

3. DATA ANALYSIS

The first step in the data analysis was to locate the sparks in real space. Then two

straight-line trajectories were fitted to the sparks from the chambers before and after the bending magnet. The momentum was then determined by integrating backwards through the magnet starting from the trajectory determined by the third and fourth chambers. This was done by an iterative method. The data were then binned according to angle (relative to the neutron beam), momentum, and time-of-flight. The proton-deuteron separation was then carried out using the momentum and time-of-flight information.

3.1. *Location of sparks*

In locating the path of a particle through a four gap spark chamber, we have a redundancy of information coming from the four wire planes oriented in four different directions. This redundancy was used to remove ambiguities in multispark events and to improve efficiency and accuracy. The information was handled in a very efficient way using a series of subroutines developed by LRL programmers [9].

Initially the spacing between the four planes in a chamber was neglected, so that the problem reduced to that of finding the intersection of an orbit in one plane rather than the more complicated problem of finding an orbit through four planes. For each event there could be zero, one, or two spark locations recorded in each plane. The first program tried all possible combinations using one wire from each plane. For each combination it calculated a point $P = (x,y)$ and its "residual" r which is a measure of the goodness of fit.

P and r were determined in the following way: each wire has the equation

$$A_i x + B_i y = C_i , \qquad i = 1, 4 , \tag{3}$$

where A_i and B_i are the direction cosines of each of the four wires. In matrix notation eq. (3) becomes

$$MP = C \tag{4}$$

where

$$M = \begin{pmatrix} A_1 & B_1 \\ A_2 & B_2 \\ A_3 & B_3 \\ A_4 & B_4 \end{pmatrix} , \qquad P = \begin{pmatrix} x \\ y \end{pmatrix} , \qquad C = \begin{pmatrix} C_1 \\ C_2 \\ C_3 \\ C_4 \end{pmatrix} .$$

However, if we try to solve for P we find the system is overdetermined and has no solution in general. Eq. (4) can be modified:

$$MP - C = r\,, \qquad \text{where} \quad r = \begin{pmatrix} r_1 \\ r_2 \\ r_3 \\ r_4 \end{pmatrix} \tag{5}$$

There exists a unique solution of eq. (5) which minimizes the sum of the squares of the residuals r_i. The solution can be written as

$$P = M^{\mathrm{I}} C\,,$$

where M^{I} is the generalized inverse of M. This equation and its solution are discussed by Rust et al. [10].

The residual r_i turns out to be the perpendicular distance from point P to the wire in plane i. If the residuals were small enough (less than $\frac{1}{2}$ inch) the corresponding wires were used in determining the orbit. If the residuals were too large, the whole program was repeated using all possible combinations of wires from each of three planes. If an acceptable solution still did not exist, two planes were used (in chamber 1 only). However two plane solutions were usually rejected for other reasons: e.g., none of the other chambers fired. In this experiment chamber one had the largest number of two wire events. It was found that almost all of these events were protons which were created or deflected in the frame of chamber one and thus did not pass through it (subsect. 3.3).

After the proper set of wire combinations was found for the four chambers, the particle orbit was calculated. The trajectory was found for the particle before it entered the magnet from chambers 1 and 2, and after it left the magnet from chambers 3 and 4. These were taken to be the straight lines which minimized the sum of the squares of the perpendicular distances to each of the 8 wires in the first (or second) pair of chambers. The solution involves solving linear equations and is straightforward [11]. The calculated straight line trajectory is given in terms of five parameters: three coordinates which designate a point through which the trajectory passes, and two slopes which give the direction of the trajectories.

The accuracy of the surveyed positions of the four chambers in the spectrometer was checked by collecting data with the magnet turned off. Particles would then go straight through all chambers without bending. The measured spark locations in the chambers should be colinear if the surveying were done accurately. The deviations were found to vary from 0.0 to 1.3 mm for the various positions. After these corrections were added, the programs were run again to verify the colinearity of the orbits.

3.2. *Momentum determination*

After the trajectory of the particle entering and leaving the magnet was calculated, the momentum of the particle was found from the bending in the magnet by successive approximations.

The first step was to find an approximate momentum P_1 from the formula

$$P_1 = (\text{correction}) \times \frac{2qBL}{\sin\alpha_{in} + \sin\alpha_{out}} . \tag{6}$$

This formula is exact without the correction term for a particle of charge q traversing a field B in a rectangular region of length L. As shown in fig. 4, α_{in} is the incoming angle and α_{out} is the outgoing angle. The correction is a polynomial with 81 parameters, c_{ijkl}:

$$\text{correction} = \sum_{i=1}^{3}\sum_{j=1}^{3}\sum_{k=1}^{3}\sum_{l=1}^{3} c_{ijkl} s_1^{i-1} s_0^{j-1} y_0^{k-1} z_0^{l-1} ,$$

where $s_1 = \tan\alpha_{in}$, $s_0 = \tan\alpha_{out}$, y_0 = zero intercept of orbit on y-axis (fig. 4), z_0 = zero intercept of orbit on z-axis.

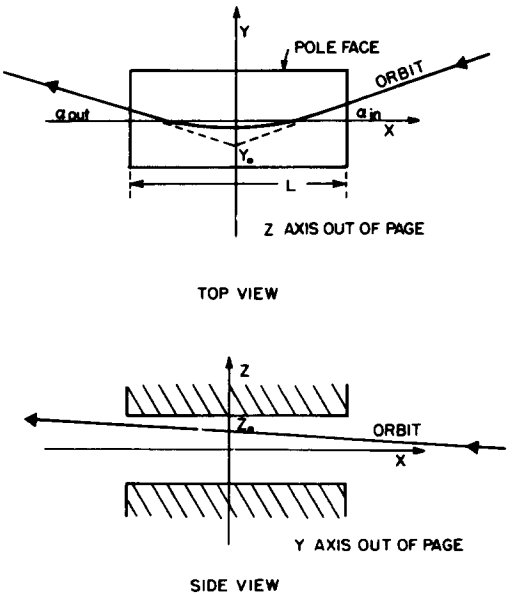

Fig. 4. Geometry of deuteron orbits.

The 81 parameters were found by generating several hundred orbits of known momentum, applying eq. (6) to each orbit, and adjusting c_{ijkl} to minimize the total RMS error.

Next a more accurate numerical integration was done. The approximate momentum P_1 was used in tracing the path of the particle through the magnetic field step by step; the orbit was bent at each step according to the direction and magnitude of the field. The value of the vertical component of the field at each point was interpolated from a lattice of 5151 field measurements; the other components were computed from div $\mathbf{B} = 0$. After the calculated orbit was clear of the field, its intersection with the next spark chamber was computed. If this intersection point was within 0.5 mm of the actual spark location, the calculation was close enough and P_1 was within 0.2% accuracy. If the intersection point was further than 0.5 mm, a second iteration was made. Eq. (6) was used again with $\sin\alpha_{\text{out}}$ determined from the integration intersection point rather than from the actual spark location. This value for P (P_{new}) gave a quantitative estimate of the difference between P_1 and the true momentum. A new trial momentum P_2 was obtained from

$$P_2 = P_1 + \Delta P ,$$

where $\Delta P = P_1 - P_{\text{new}}$. Another integration was then done with P_2 to check it. In almost all cases no more than two integrations were needed to obtain the desired accuracy. The average computer time per event was 0.2 sec at the LRL 6600 computer.

In the orbit integration process only three chambers were needed. Two were used to find the incoming orbit, and one was used to check the intersection point of the outgoing orbit. This was useful if one of the chambers did not fire. Also the unused chambers provided a final systematic check of the accuracy of the spectrometer in the following manner: The computer orbit was projected to the unused chamber, and the deviation from the actual spark location was plotted in a histogram. These distributions had displacements ranging from −0.6 to 1.8 mm for the nine magnet positions. The resulting systematic errors are discussed in subsect. 4.2. The width at half maximum varied from 5 to 6 mm. This corresponds to a spread in the momentum measurement of approximately 2.0%, which agrees with the spread in momentum expected from multiple Coulomb scattering in the spectrometer.

The solid angle or detection efficiency Eff(θ,P) of the deuteron spectrometer was computed for each of the 9 magnet settings. The computations involved numerical integrations over the surface of counter D_1, which controlled the angular acceptance of the deuteron, and over the surface of D_2, which determined the acceptance of the deuteron momentum. The finite target size and the spatial distribution of the neutrons in the beam were also considered in the calculation. The incident neutron spectrum and the effects of Coulomb scattering were introduced at a later stage of the analysis (subsect. 3.6).

For consistency in the data analysis the same criteria used in the integration were

used to reject events. If an event fell outside the integration boundaries ("fiducial volume"), the event was rejected. The fiducial volume was made to be smaller than that determined by the counters and pole faces – small enough so that no events were lost through Coulomb scattering or through an inaccuracy in the solid angle calculation. In the course of the data analysis histograms and scatter plots were made to compare computed orbits with actual orbits to make sure the fiducial volume was small enough, but no smaller than necessary.

3.3. *Data processing and binning*

In the first step of the data reduction the raw data tape from the PDP-5 on-line computer was processed on the LRL Control Data 6600 computer. The magnetostrictive scaler readings were translated into spatial coordinates. The spark locations and orbits were found and orbit integrations through the magnet performed to obtain the momentum. The orbits, momenta, time of flight, monitor counters, and other data for the half million events were recorded on fifty reduced data tapes.

Next the reduced data tapes were run to set and check the fiducial volume. The orbits were projected back to the target to check the size, location, and intensity distribution of the beam. The reduced data tapes were then run again, and the parameters of the good events which fell inside the fiducial volume were stored in histograms (bins). The fate of the events in the fiducial cut are tabulated for a typical run in table 1.

Table 1
Disposition of events in fiducial cut

	Events with four chambers	Events with missing chambers			
		#1	#2	#3	#4
Good events	7030	1	5	44	12
Hit pole face	845	0	0	2	1
θ too large	26	0	0	1	0
θ too small	282	0	0	0	0
P too large	67	0	0	1	0
P too small	1049	0	1	9	66
Outside target	1121	160	0	2	0
Misc. rejects	39	0	0	0	1
	10459	161	6	59	80

Of the 10 765 events in this sample, 33% were rejected in the fiducial cut. Of the good events only 1% had a chamber that did not fire. On this basis it was estimated that $\ll 0.1\%$ were lost because two chambers did not fire. The relatively low efficiency of chamber 1 for events which were "outside the target" is due to the fact that some particles were created in the chamber frame which was very close to the neutron beam.

It was found that typically 1.2% of the triggers did not have enough sparks to determine the orbits. These were mostly accidental triggers or stray particles which did not pass through some of the chambers. The orbit integration failed for 2.7% of the events. This was due mostly to particles which deflected from the magnet pole face. Otherwise it was due to large angle scatterings elsewhere in the spectrometer.

The events were binned in three dimensions according to angle, momentum, and time of flight. After all the data were binned, the separation of the protons and deuterons was made as discussed in the next section.

The bin sizes were as follows: 26 angle bins $\frac{1}{4}^\circ$ wide, 45 momentum bins 20 MeV wide, and 30 TOF bins 1 nsec wide. This makes a total of 35100 bins. Word packing techniques had to be used to fit this into the computer memory and still leave room for the rest of the program. This procedure is described in detail in the next section.

The binned data from each of the fifty data tapes were punched on cards. There were nine separate decks of cards corresponding to the nine magnet positions. The same procedure was followed for the target empty runs.

3.4. *Separation of protons and deuterons*

The timing requirements in the trigger were purposely kept loose to insure that no deuterons were lost. The event sample therefore included a large contamination of protons. The mass of each particle could be calculated from its momentum and TOF. For low momentum particles it was possible to separate the deuterons from the protons, but the timing resolution of ± 1 nsec made it impossible to completely resolve high momentum particles. Fig. 5 shows typical histograms for a case with relatively good and relatively poor separation. Therefore a single event could not always be unambiguously determined to be a proton or a deuteron.

The shapes of the histograms in all cases were found to fit two separated gaussian functions to a high accuracy. Thus gaussian shapes were fitted to the data and the area of each gaussian respectively gave the number of protons and deuterons for that bin. The fitting procedure made use of the method of maximum likelihood. In summary the separation proceeded as follows:

(1) An abbreviated form of the 35 100 bins was printed out.

(2) A representative sample of angle and momentum bins were chosen. For each of these bins the time-of-flight histogram was plotted. The locations of the peaks of the deuteron gaussians were measured by eye to within 0.2 nsec accuracy to give a first approximation.

(3) A function with seven parameters was fitted to this sample to give the gaussian peak location as a function of angle and momentum.

(4) The average deuteron gaussian width was measured. (It was fairly independent of angle and momentum.)

(5) A polynomial with four parameters was added as a correction to the function in step 3. It had the form $C = a_1 + a_2\theta + a_3 P + a_4 P\theta$, where θ and P are the lab angle and momentum.

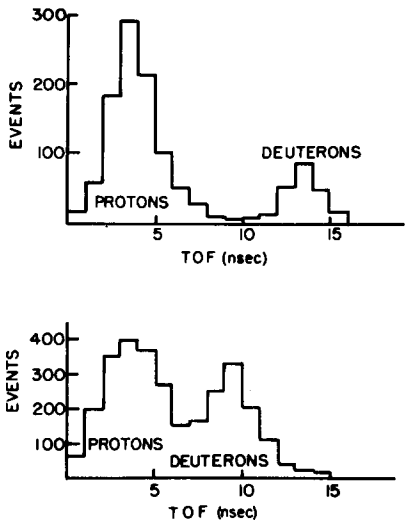

Fig. 5. Typical histograms for the time-of-flight. In the first case the proton and deuteron peaks are well separated; the second shows a situation with poor separation.

(6) A polynomial with four parameters was added as a correction to the average width in step 4. It has the same form: $C' = b_1 + b_2\theta + b_3P + b_4P\theta$.

(7) The location of the proton gaussian (as a function of deuteron width and location) could be found exactly using maximum likelihood, and its width could be found using a very good approximation.

(8) The eight parameters a_i and b_i were adjusted to maximize the likelihood of the fit of the data by the method of steepest ascent. For this fit the number of deuterons were calculated for each bin.

(9) An eight-dimensional ellipsoid was computed in the (a_i,b_i) space such that the probability was one-half maximum on its surface. For each angle-momentum bin this ellipsoid was projected onto the two-dimensional subspace: width versus location of the gaussian. This projection is an ellipse.

(10) For each point on this second ellipse, the number of corresponding deuterons could be computed. The maximum and minimum give the separation error.

This procedure allowed the gaussian parameters (width and location) to vary until the most likely fit was found, with the constraint that the variation be smooth from bin to bin.

In two of the magnet positions (one with poor separation and one with good separation) it was found that the proton-deuteron separation error was about 1% of the statistical error. Therefore steps 9 and 10 were dropped for the remaining seven positions.

Table 2 shows the disposition of the events for the nine magnet positions. The table shows the numbers of deuterons remaining after the fiducial cuts discussed

Table 2
Disposition of events (in thousands)

Magnet position	Total triggers	Number surviving fiducial cut	Deuteron events after eliminating protons
1	198	124	50
2	16	6	3
3	12	6	3
4	36	27	11
5	44	19	12
6	38	20	17
7	40	24	9
8	50	5	3
9	48	5	3
Total	482	236	111

previously were applied and protons eliminated. Positions 8 and 9 covered small deuteron angles and counter D_1 was in the neutron beam. Most of the triggers were for charged particles created in that counter.

3.5. *Other corrections*

After the deuterons were separated from the protons, other corrections were applied. These were for energy loss and Coulomb scattering of the deuteron in passing through the target and spectrometer, contamination from the reaction $np \to \gamma d$, events originating in the walls of the target, absorption of deuterons, and $(d+2\pi)$ production. These corrections were incorporated in the Monte Carlo simulation described in the next section.

Energy loss

The energy loss as a function of deuteron momentum was calculated using an LRL program [12]. The thicknesses of the various absorbing materials were put into the program. The mean energy loss and energy loss distribution were calculated using Bethe's stopping power formula [13]. The width of the distribution was found to be much smaller than the resolution of the spectrometer, and therefore was neglected. The result of the energy loss correction is a small addition of momentum to the value measured by the spectrometer. The correction ranged from 5% at low momenta to 0.8% at higher momenta.

Multiple Coulomb scattering

Multiple Coulomb scattering caused an uncertainty in the measurement of the deuteron angle. The deviation of the true value of θ from the measured value has an approximately gaussian distribution. The projected width $\Delta\theta$ is given by the equation [14]:

$$\Delta\theta = \frac{15 \text{ MeV}}{pv}\sqrt{\frac{L}{L_{\text{rad}}}}$$

where p and v are the momentum and velocity of the particle, L is the thickness of the absorber, and L_{rad} is the radiation length of the material.

This effect shows up in the data in two ways. First it causes an error in the laboratory polar angle due to the scattering material between the target and second spark chamber. Second it causes an error in the measurement of momentum due to scattering of the orbit in passing through the spectrometer. To minimize the error in the momentum the orbit integration was done using chambers 2, 3, and 4 rather than chambers 1, 2 and 3 because the first combination had less material.

$np \rightarrow \gamma d$

The differential cross section for $np \rightarrow \gamma d$ was obtained from the time reversed photodisintegration reaction $\gamma d \rightarrow np$ [15]. The principle of detailed balance was used to transform the cross section to that for $np \rightarrow \gamma d$. Although the cross section for pion production is about 100 times that for gamma production, there are regions where the kinematics enhances the gamma rate and suppresses the pion rate. Consequently the gamma contamination ranged from 0.02% to 20.0% depending on the kinematic region.

Target empty correction

To correct for events coming from the target walls, about six percent of the data were taken with the target empty. These events were processed in the same way as the target full events. They were normalized using the monitor counters so that the number of incoming neutrons corresponded to that for the target full. This correction ranged from 4% to 18% for the nine magnet settings.

Deuteron absorption

Some deuterons were lost in passing through the target and spectrometer due to nuclear scattering and absorption. Deuterons which are stripped or which scatter elastically in the target or spectrometer would generally be lost, so the correction was based on the total cross section. The total cross section for a deuteron-nuclear interaction is strongly momentum dependent for our range of momenta. The total cross sections for deuterons on nuclei of atomic number A were obtained by adding the neutron and proton total cross sections multiplied by a screening factor [16]:

$$\sigma(dA) = [\sigma(nA)+\sigma(pA)] \times 0.97 .$$

The total neutron and proton cross sections come from the empirical formula [16]:

$$\sigma(nA) = [(A-Z)\sigma(pp) + Z\sigma(np)]\,[1-0.155A^{0.26}] ,$$

$$\sigma(pA) = [(A-Z)\sigma(np) + Z\sigma(pp)]\,[1-0.155A^{0.26}] .$$

The data for $\sigma(np)$ and $\sigma(pp)$ were taken from ref. [17].

The total cross sections for deuterons on nuclei have been measured in our momentum range only at 700 MeV/c [18]. This value agrees with the empirical formulas to about 15% accuracy. The corrections for absorption varied from a maximum of 4% at 800 MeV/c to 1.4% at 1400 MeV/c; the uncertainty in the correction therefore has a small effect on the cross sections.

$np \to d\pi\pi$

The threshold for $np \to d\pi\pi$ is about 580 MeV. Although our maximum beam energy is above this threshold, on the basis of available data [19] the cross section for two pion production at 700 MeV is estimated to be less than 0.2% that for one pion production. Two pion production was therefore neglected.

3.6. *Cross section calculation*

The differential cross section is most conveniently expressed as a function of θ^* and E where θ^* is the center of mass angle between the deuteron and neutron beam, and E is the incident neutron energy. The raw data can be converted to a differential cross section using the Monte Carlo basic formula:

$$d\sigma(\theta^*,E) = \frac{N_{expt}(\theta^*,E)}{N_{gen}(\theta^*,E,d\sigma_{est})} d\sigma_{est}(\theta^*,E)\,, \tag{7}$$

where N_{expt} is the measured number of events in a small bin centered at θ^* and E with target empty events subtracted; $d\sigma_{est}$ is an estimate of the differential cross section; and N_{gen} is the calculated number of events in the same bin assuming $d\sigma_{est}$ in the calculation. Eq. (7) can be iterated by replacing $d\sigma_{est}$ with $d\sigma$ and repeating the calculation. It converges so rapidly that only two iterations were necessary.

The calculation of N_{gen} usually involves a Monte Carlo simulation of the experiment in which the solid angle is also implicitly calculated. In this case it was faster and more accurate to generate events uniformly rather than randomly, and to compute the solid angle separately as discussed in subsect. 3.2 above.

The determination of N_{gen} proceeded as follows: simulated events were generated in the c.m.s. with θ^* running from 0° to 180° in 225 steps 0.8° apart, and with E running from threshold to 720 MeV in 120 steps 4 MeV apart. The number of events generated at each value of θ and E was proportional to

$$F = d\sigma_{est}(\theta^*,E)\ \mathrm{Eff}(\theta,P)\ \mathrm{D}(E)\ M\ \mathrm{Norm}\ T$$

where $\mathrm{Eff}(\theta,P)$ is the geometric detection efficiency (subsect. 3.2); $D(E)$ is the neutron energy distribution normalized to unity; M is the number of counts in the beam monitor scaler; and T is the number of protons per barn in the target. Norm is the normalization which relates M to the number of neutrons in the beam. Norm was determined from the $np \to \gamma d$ experiment with about a 20% uncertainty (sect. 2). The events generated in this manner were grouped into bins to form N_{gen}.

The Coulomb scattering of both the laboratory polar angle and momentum was

folded into the generated events, and the energy loss experienced by the deuterons was also simulated. Finally the simulated events were binned in c.m. coordinates. The correction for contamination from dγ production described earlier was included in N_{gen} by generating events using eq. (7), except that $d\sigma_{est}$ was replaced by the cross section for dγ production.

Also implicitly included in the calculation of N_{gen} was its double-valued nature. In some kinematic regions there are two values of (θ^*,E) which correspond to each value of the laboratory coordinates (θ,P). Thus a bin in lab space will contain contributions from two distinct c.m. coordinate regions in the c.m.s. corresponding to incident neutrons of two different energies. In fig. 6 the cross-hatched area is the ambiguous kinematic region. In the ambiguous area both N_{expt} and N_{gen} are a composite of the two kinematic regions, so that $d\sigma$ from eq. (7) is the sum over these two regions, rather than being a direct measurement of the cross section in either. However, most of the data is not ambiguous because in one of the c.m. regions there are no incident neutrons of sufficient energy to cause the confusion.

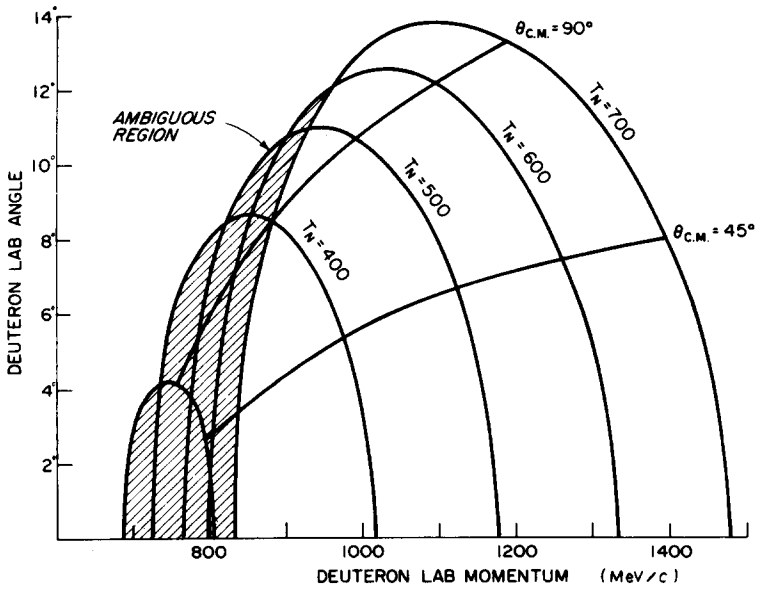

Fig. 6. Deuteron kinematics for incident neutrons of various energies. Events with deuterons in the shaded region have two possible solutions for the incident neutron energy and c.m.s. angle.

Table 3
Angular distributions normalized to an area $2\pi \times 1000$

Angle (c.m.)	Energy (MeV) 325	375	425	475	525	575	625	675
5°	1046 ±210	1120 ±84	997 ±77	663 ±75	687 ±101	983 ±273	704 ±203	–
15	814 ±81	942 ±41	824 ±27	917 ±33	938 ±38	1097 ±53	804 ±41	835 ±55
25	801 ±75	766 ±50	803 ±33	802 ±35	858 ±32	925 ±34	901 ±52	807 ±55
35	899 ±64	803 ±65	833 ±63	764 ±41	757 ±34	761 ±29	748 ±46	655 ±40
45	684 ±56	767 ±57	653 ±34	612 ±29	637 ±29	667 ±33	660 ±28	636 ±24
55	491 ±34	560 ±39	493 ±25	500 ±25	505 ±24	513 ±25	552 ±23	574 ±18
65	396 ±30	427 ±41	434 ±34	446 ±26	399 ±27	420 ±20	439 ±18	430 ±16
75	319 ±22	330 ±43	314 ±21	333 ±20	316 ±17	270 ±11	281 ±11	317 ±7
85	220 ±18	238 ±18	327 ±29	273 ±16	259 ±12	242 ±10	232 ±10	267 ±7
95	195 ±20	289 ±12	354 ±42	279 ±34	242 ±16	219 ±11	236 ±13	267 ±13
105	269 ±34	265 ±21	322 ±27	377 ±54	352 ±73	320 ±49	317 ±32	344 ±18
115	420 ±60	366 ±48	383 ±37	426 ±24	440 ±28	455 ±65	466 ±67	443 ±34
125	805 ±307	369 ±60	517 ±155	564 ±168	634 ±147	572 ±130	557 ±110	565 ±77
135	–	780 ±364	628 ±82	648 ±87	616 ±51	656 ±41	614 ±43	658 ±66
145	890 ±126	1309 ±348	781 ±85	724 ±74	769 ±57	715 ±44	838 ±88	825 ±109
155	872 ±112	713 ±188	955 ±152	729 ±102	984 ±101	879 ±69	904 ±77	1188 ±320
165	952 ±190	999 ±113	863 ±71	871 ±64	821 ±68	884 ±76	875 ±61	852 ±98
175	–	–	–	1417 ±457	1067 ±244	956 ±118	1048 ±212	757 ±91

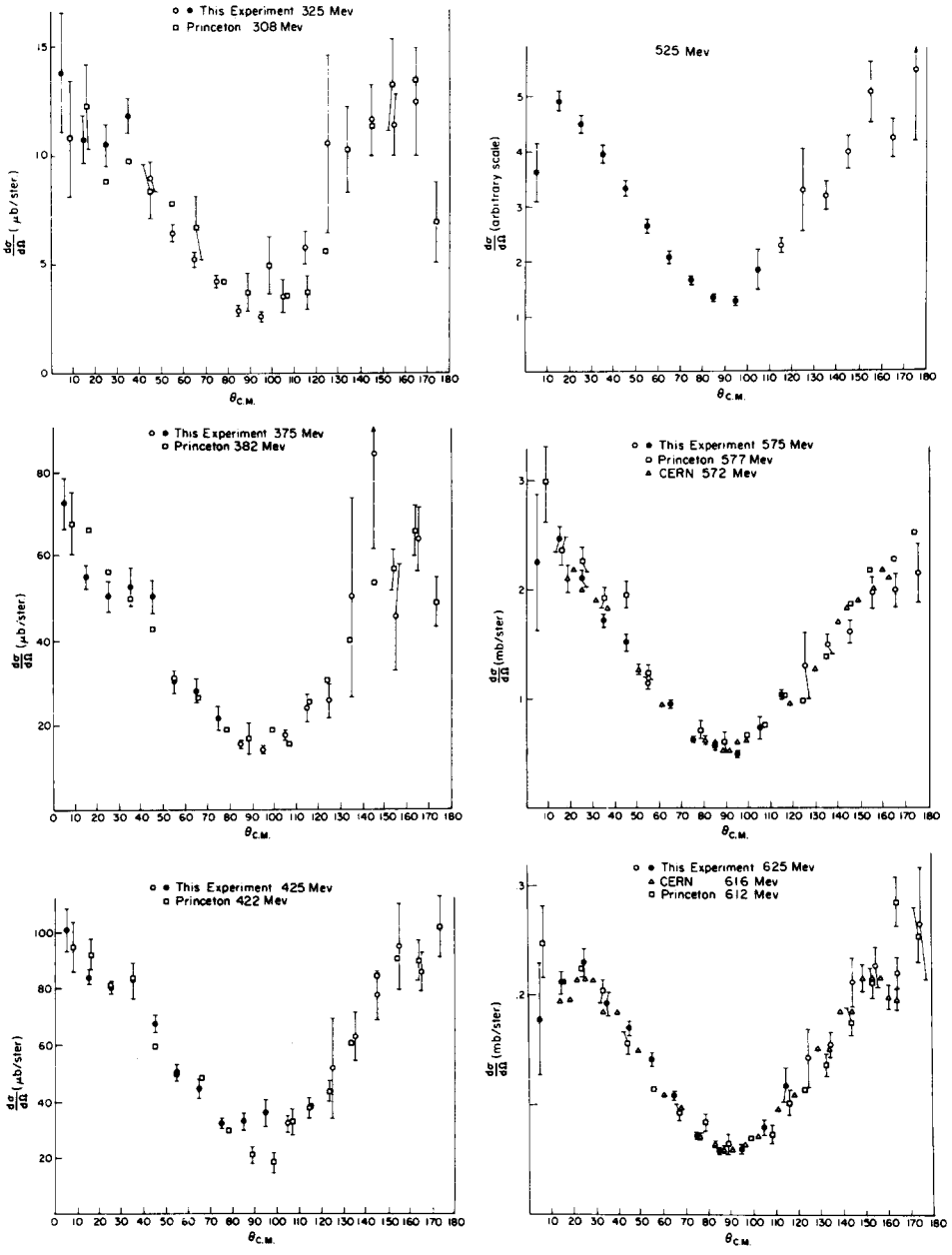

Fig. 7. For text see next page.

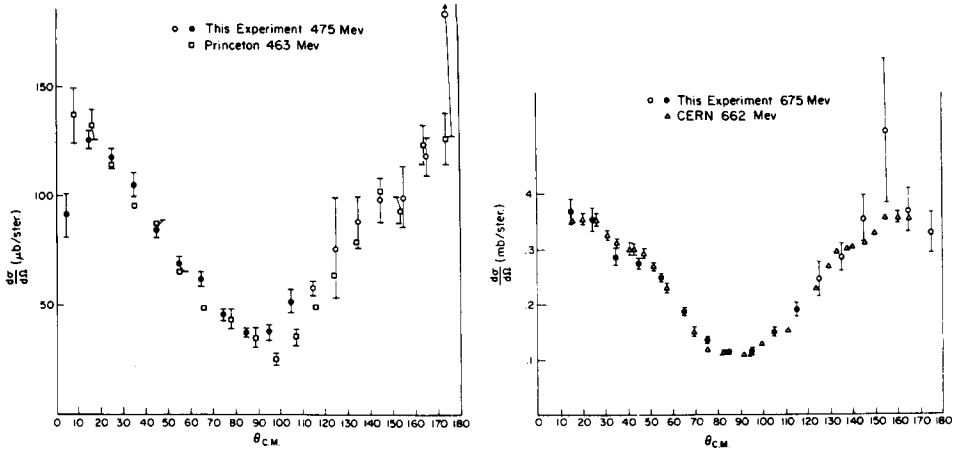

Fig. 7. Results for the differential cross section normalized to the CERN [20] and Princeton [21] data. The CERN data plotted are $\frac{1}{2}\sigma(pp \rightarrow \pi^+ d)$ obtained from the inverse using detailed balance.

4. RESULTS

4.1. *Cross sections*

Our results for the cross sections are given in table 3. The data are in 8 energy bins, 50 MeV wide, from 300 to 700 MeV; and 18 angle bins, 10° wide, from 0° to 180°. The data from each energy is normalized such that the area is $2\pi \times 1000$. The data are plotted in fig. 7. Points in the ambiguous region are plotted as open circles. Results from CERN [20] and Princeton [21] are shown as well; however only a few typical errors are displayed for clarity. The CERN data comes from measurements of $\pi^+ d \rightarrow pp$, transformed to $pp \rightarrow d\pi^+$ using detailed balance, and then divided by 2 to normalize to $np \rightarrow d\pi^0$. The CERN data covers an angular range from 90° to 180°. It is reflected about 90° and plotted twice. The Princeton results come from a measurement of the same reaction at this experiment. In the plots our data is normalized to fit the Princeton and CERN results since there is a large uncertainty in our total cross section.

4.2. *Systematic errors*

The alignment of the spark chambers was found to have a maximum inaccuracy of about 1.3 mm. This would give a maximum systematic error in the deuteron angle measurement of about 0.05°. The maximum systematic error in the momentum measurement is about 0.5%. The systematic error in the cross section was estimated by varying the lab angle of the deuteron by ±0.05°, and the momentum by ±0.5%, and then recomputing the various cross sections. The resulting variations of the cross

sections were combined with the statistical errors to obtain the errors quoted in table 3. The systematic errors are about $\frac{1}{3}$ of the statistical errors in the non-ambiguous region, but in the ambiguous region the systematic errors dominate and are rather large.

4.3. *Coefficients*

To conform to the practice of other NN $\rightleftharpoons$ πd experiments, we fit the cross sections to the function

$$\sigma(\theta^*) \propto A + \cos^2\theta^* + B\cos^4\theta^* . \tag{8}$$

Our A and B coefficients are plotted as a function of energy in fig. 8 along with the $\pi^+ d \rightarrow pp$ results from CERN. There are a number of other experiments measuring the reactions NN $\rightarrow$ πd, but only the CERN experiment was sufficiently accurate to determine the coefficient of the $\cos^4\theta^*$ term.

Our cross sections were also fitted to the function:

$$\sigma(\theta^*) \propto A' + U\cos\theta^* + \cos^2\theta^* + B'\cos^4\theta^* . \tag{9}$$

If isotopic spin invariance is not violated, the coefficient U should vanish. Table 4

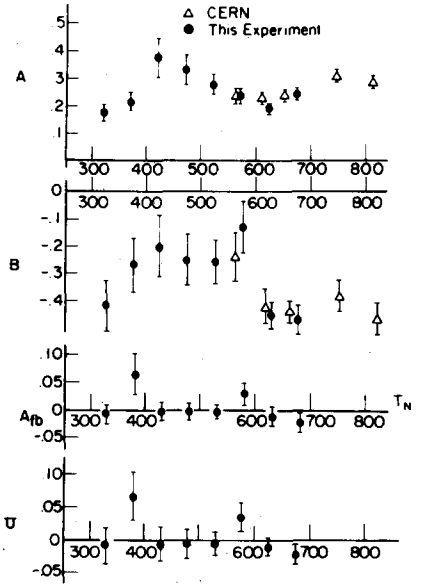

Fig. 8. The A and B coefficients, the fore-aft asymmetry A_{fb}, and the coefficient of the $\cos\theta^*$ term U.

Table 4
Coefficients

(MeV)	A	B	χ^2 per deg. of freedom	U	A_{fb}
325	0.171 ± 0.031	−0.412 ± 0.094	13.6/14	−0.007 ± 0.027	−0.8 ± 2.1%
375	0.209 ± 0.033	−0.263 ± 0.099	25.5/15	+0.066 ± 0.038	6.5 ± 3.8
425	0.379 ± 0.076	−0.199 ± 0.122	17.5/15	−0.007 ± 0.027	−0.5 ± 1.9
475	0.335 ± 0.052	−0.254 ± 0.094	19.8/17	−0.006 ± 0.022	−0.5 ± 1.8
525	0.274 ± 0.034	−0.253 ± 0.084	15.5/16	−0.007 ± 0.019	−0.6 ± 1.6
575	0.242 ± 0.028	−0.130 ± 0.097	20.7/16	+0.033 ± 0.022	2.9 ± 1.9
625	0.189 ± 0.018	−0.452 ± 0.051	15.0/16	−0.012 ± 0.014	−1.4 ± 1.6
675	0.247 ± 0.021	−0.474 ± 0.057	13.1/15	−0.023 ± 0.016	−2.4 ± 1.7

shows that U is consistent with zero. Table 4 also gives the values of the other coefficients along with the χ^2 for the fit. The forward-backward asymmetry is defined as

$$A_{fb} = \left[\int_0^{\frac{1}{2}\pi} \sigma d\Omega - \int_{\frac{1}{2}\pi}^{\pi} \sigma d\Omega\right] \Big/ \left[\int_0^{\frac{1}{2}\pi} \sigma d\Omega + \int_{\frac{1}{2}\pi}^{\pi} \sigma d\Omega\right], \tag{10}$$

and is shown in fig. 8; A_{fb} serves as an important measure of the isospin-violating amplitudes as discussed below.

A fit to the function

$$\sigma(\theta^*) \propto A' + \cos^2\theta^*$$

gave a much larger χ^2 than that for eq. (8). Thus the B coefficient is necessary for a fit to this experiment.

4.4. *Comparison with other experiments*

As discussed in sect. 1 the invariance of the strong interaction with respect to the third component of isospin leads to the result that the angular distribution of $pp \to \pi^+ d$ and $np \to \pi^0 d$ are the same.

The CERN $\pi^+ d \to pp$ experiment is the only $NN \rightleftharpoons \pi d$ experiment which has comparable accuracy to our experiment. There is very good agreement for our results with that of CERN for both the A and B coefficients as shown in fig. 8. Our data is also consistent with all other $NN \rightleftharpoons \pi d$ experiments though the accuracies of their B coefficients are poor enough that this is not a very fruitful comparison. A summary of these other experiments can be found in ref. [20].

The agreement of the coefficients was studied at the three energies for which the CERN experiment and ours overlap. Good agreement was found. Table 5 gives limits on the differences between the coefficients from the two experiments for a 90% confidence level.

Table 5
Maximum discrepancy between A and B coefficients from $np \to \pi^0 d$ and $pp \to \pi d$ (90% confidence level).

Energy (MeV)	Maximum difference in A	Maximum difference in B
575	<9.5%	<6.3%
625	<8.5%	<4.3%
675	<7.8%	<3.5%

The Princeton experiment has measured the angular distribution for the same reaction as our experiment in the same energy range [21]. Their systematic errors are too large to allow them to detect the B coefficient. Their measurement of the asymmetry A_{fb} is consistent with zero, but their errors are more than four times ours.

4.5. *Total cross section*

In order to measure the total cross section, we must know the absolute flux of neutrons at each energy in terms of monitor counts. This was determined using the $np \to \gamma d$ data as discussed in sect. 2. The distribution in fig. 2 does not show the errors which range from 40% at low energies to 20% at higher energies. This will cause an equally large error in our measurement of the total cross section.

The total cross section is shown in fig. 9 along with the total cross section for $pp \to \pi^+ d$ which is indicated by a band to show the uncertainty in the measurement. The cross sections are consistent, but the uncertainties are too large for the comparison to be of much value.

4.6. *Comparison with theory*

There are a number of theoretical models for the reaction $NN \rightleftharpoons \pi d$. The most successful is a covariant theory by Schiff and Tran Thanh Van who calculate the singularity structure of the scattering amplitude using dispersion relations for the partial wave amplitudes [22]. They also give a summary of other models. The theories previous to this are unsatisfactory for our purposes because they do not consider higher-order partial waves for which this experiment is sensitive.

If we consider only s and p waves in the final state, the allowed transitions and their angular distributions are the following:

Transition amplitude	Angular distribution
$a = ({}^3P_1 \to {}^3S_1)$	Isotropic
$b = ({}^1S_0 \to {}^3P_0)$	Isotropic
$c = ({}^1D_2 \to {}^3P_2)$	$\frac{1}{3} + \cos^2\theta^*$

All models predict that c is the dominant amplitude. This agrees with most experiments; the angular distributions are roughly $0.25 + \cos^2\theta^*$ within a 6% to 20%

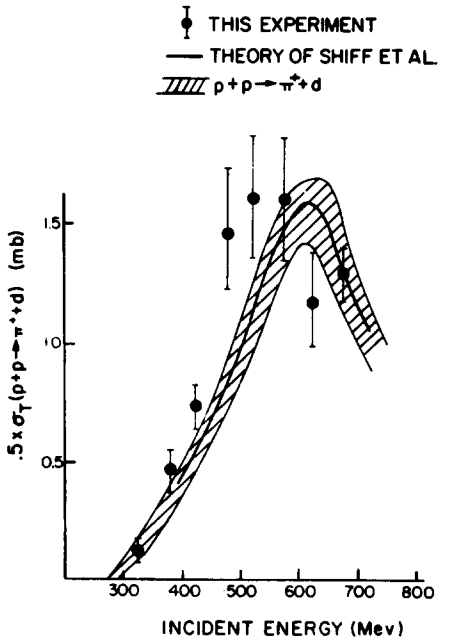

Fig. 9. Comparison of np → π^0d total cross sections from this experiment with $\frac{1}{2}\sigma$(pp→π^0d), and the theoretical cross sections obtained by Schiff and Van [22].

experimental error. Furthermore, in transition c the pion angular momentum is parallel to both nucleon spins and allows an intermediate πN $(\frac{3}{2},\frac{3}{2})$ resonant state corresponding to the $\Delta(1236)$ resonance. The $\Delta(1236)$ would appear as a peak in the total cross section at 600 MeV incident neutron energy. Experiments confirm a strong peak in that region (fig. 9).

Schiff and Van consider higher order partial waves also. The important waves are those that interfere with the dominant transition $^1D_2 \rightarrow {}^3P_2$. These transitions are:

$$d = ({}^3F_2 \rightarrow {}^1D_2)\,,$$

$$e = ({}^3F_4 \rightarrow {}^1G_4)\,.$$

The results of their analysis show that a and d are negligible, and $b \approx e \approx c/10$. They find that a fourth power $\cos\theta$ term is important and is the same order of magnitude as the $\cos^2\theta$ term. Theirs is the only theory which predicts the values of the B coefficients. Rather than giving their results in terms of the A and B coefficients, they plot their derived angular distributions at several energies. The coefficients were obtained by fitting eq. (8) to their plots. The results of this fit are given in table 6.

Table 6
A and B coefficients in theory of Schiff and Van [22].

Energy (MeV)	A	B
460	0.87	0.66
572	0.61	0.50
633	0.54	0.47
690	0.49	0.43
745	0.45	0.40

Our experimental results have the same magnitude, but the opposite sign for the B coefficients. No attempt will be made here to try and explain this discrepancy because the significance of the B coefficients is obscurely imbedded in the theory – they result primarily from an interference of higher order partial waves with the dominant transition.

The theory is much more successful in deriving the total cross section. This theory and the experimental measurements of the total cross section are shown in fig. 8.

If isospin invariance is violated, it has been shown [21] that the important violating amplitudes (transitions from $I = 0$ to $I = 1$) can be

$$f = ({}^1P_3 \to {}^3S_1)$$

$$g = ({}^1P_1 \to {}^3D_1)$$

$$h = ({}^1F_3 \to {}^3D_3) .$$

These transitions give rise to odd powers of $\cos\theta$ in angular distribution. Moreover, the ratio of the real part of the violating to the dominant nonviolating amplitude $({}^1D_2 \to {}^3P_2)$ is given by [21]

$$\mathrm{Re}\left(\frac{f}{c}\right) = 2^{-\frac{1}{2}} A_{\mathrm{fb}} ; \qquad \mathrm{Re}\left(\frac{g}{c}\right) = 4A_{\mathrm{fb}} ; \qquad \mathrm{Re}\left(\frac{h}{c}\right) = 6^{-\frac{1}{2}} A_{\mathrm{fb}} .$$

Since the average value of our measurement of A_{fb} is only $-0.36 \pm 0.66\%$, we have set a tight upper limit on the real part of the isospin violating amplitude. To the extent that A_{fb} is a measure of the ratio of the violating to the nonviolating amplitude, this limit ranges from 0.27% to 2.6% depending on which isospin-violating amplitude is assumed.

5. CONCLUSIONS

Isospin invariance has previously been tested in several experiments involving pions and light nuclei. (See sect. 1 for a summary.) These tests show that isospin is

conserved to at least 5%. The recent experiment at Princeton [21] results in a forward-backward asymmetry of 1 ± 3% in the angular distribution of the reaction $np \to \pi^0 d$. Our results show an average asymmetry of 0.36 ± 0.66% in the same reaction.

Our angular distribution agrees well with all other $NN \rightleftharpoons \pi d$ experiments. In fitting the cross section to the formula

$$\sigma(\theta^*) \propto A + \cos^2\theta^* + B\cos^4\theta^* ,$$

we and CERN [20] find consistently negative values for B with a sharp negative drop above 600 MeV. The angular distributions for these two experiments agrees within 4% to 9%. Evidence from the forward-backward asymmetry shows that transitions which do not conserve isospin do not occur to within about 1.0% accuracy – the level at which electromagnetic violations might be expected to occur.

The experimental design and set-up involved the collaboration of many people. Among these were David Cheng, Victor Perez-Mendez, Leonard Proehl, and John Sperinde from the Lawrence Radiation Laboratory; and Roy Haddock from UCLA. Their assistance is gratefully acknowledged. The 184-inch Cyclotron crew gave us excellent support throughout the experiment. We are grateful to the Lawrence Radiation Laboratory programmers for their valuable assistance in the data analysis.

REFERENCES

[1] B.L.Schrock, J.-F.Detoeuf, R.P.Haddock, J.A.Helland, M.J.Longo, K.K.Young, S.S.Wilson, D.Cheng, J.Sperinde and V.Perez-Mendez, UCRL 19350 (Sept. 1969); Proc. of the 3rd Int. Conf. on high energy phys. and nucl. structure, S.Devons, ed., Plenum Press, 1970.
[2] A.A.Carter, K.F.Riley, R.J.Tapper, D.V.Bugg, R.S.Gilmore, K.M.Knight, D.C.Salter, G.H.Stafford, E.J.N.Wilson, J.D.Davies, J.D.Dowell, P.M.Hattersley, R.J.Homer and A.W.O'Dell, Phys. Rev. 168 (1968) 1457.
[3] W.Galbraith, E.W.Jenkins, T.F.Kycia, B.A.Leontic, R.H.Phillips, A.L.Read and R.Rubinstein, Phys. Rev. 138 (1965) B913.
[4] J.A.Poirier and M.Pripstein, Phys. Rev. 130 (1963) 1171.
[5] K.R.Greider, Phys. Rev. 122 (1961) 1919.
[6] A.V.Crewe, E.Garwin, B.Ledley, E.Lillethun, R.March and S.Marcowitz, Phys. Rev. Lett. 2 (1969) 269.
[7] D.Hartig, J.C.Kluyver, A.Kusumegi, R.Rigopoulos, A.M.Sachs, G.Tibell, G.Vanderhaeghe and G.Weber, Phys. Rev. 119 (1960) 1716.
[8] V.Perez-Mendez, T.J.Devlin, J.Solomon and T.F.Droege, Nucl. Instr. 46 (1967) 197.
[9] R.Hinkins, T.Schaefer and L.Wilson, private communication.
[10] B.Rust, W.R.Birrus and C.Schneeberger, Commun. ACM (USA) 9 (1965) 381.
[11] Program "LINERR", R.Hinkins, private communication.
[12] H.Bichsel, UCRL 17538 (1967), unpublished.
[13] H.Bethe, Quantenmechanik der ein- und zwei Elektronenprobleme, in Handbuch der Physik, Vol. 24-1, 2nd ed., Springer, 1933.

[14] D.M.Ritson, Techniques of high energy physics, Interscience, 1961.
[15] R.L.Anderson, R.Prepost and B.H.Wiik, Phys. Rev. Lett. 22 (1969) 651.
[16] E.F.Parker, H.R.Gustafson, L.W.Jones, M.J.Longo, P.V.Ramana-Murthy, F.E.Ringia and B.Cork, Phys. Lett. 31B (1970) 246;
E.F.Parker, T.Dobrowolski, H.R.Gustafson, L.W.Jones, M.J.Longo, F.E.Ringia and B.Cork, Phys. Lett. 31B (1970) 250.
[17] R.Wilson, The nucleon-nucleon interaction, Interscience, 1963.
[18] G.P.Millburn, W.Birnbaum, W.E.Crandall and L.Schechter, Phys. Rev. 95 (1954) 1268.
[19] J.G.Rushbrooke, D.V.Bugg, A.J.Oxley, J.A.Zoll, M.Jobes, J.Kinson, L.Riddiford and B.Tallini, Nuovo Cim. (10) 33 (1964) 1509.
[20] C.Richard-Serre, W.Hirt, D.F.Measday, E.G.Michaelis, M.J.Saltmarsh and P.Skarek, Nucl. Phys. B20 (1970) 413.
[21] D.F.Bartlett, C.E.Friedberg, K.Goulianos, I.S.Hammerman and D.P.Hutchinson, Phys. Rev. D1 (1970) 1984.
[22] D.Schiff and J.Tran Thanh Van, Nucl. Phys. B5 (1968) 529.